Manipulation of Zn deposition Behavior to Achieve High-rate Aqueous Zinc Batteries *via* High Valence Zirconium Ions

Zhuo Chen, [a] Junrun Feng, [*, a] Weihua Zhou, [a] Jun Lu, [a] Jinlong Cai, [a] Lun Zhang, [b] Lin Sheng, [c] Hao Gu, [b] Pengfei Yao, [a] Feng Ryan Wang, [b] Zhangxiang Hao[*, a]

[a] School of Science, School of Chip Industry, Hubei University of Technology, Wuhan, Hubei 430068, China

[b] Materials and Catalysis Laboratory, Department of Chemical Engineering, University College London, London WC1E 7JE, United Kingdom

[c] School of Mechanical and Electronic Engineering, Suzhou University, Suzhou, Anhui 234000, China

*Corresponding author. E-mail: fengjunrun@hbut.edu.cn; haozx@hbut.edu.cn

Keywords: aqueous zinc ions battery, electrolyte additive, Zn deposition, high valence ions, zirconium acetate

Abstract: Aqueous zinc ion batteries (AZIBs) are excellent energy storage devices with high safety and low cost. However, the corrosion reaction and zinc dendrites formation occur on the surface of zinc anodes are hindering their further development. To solve

the problems, zirconium acetate (ZA) was used as an electrolyte additive in the $ZnSO_4$ electrolyte. Attributing to the higher electro-positivity of Zr^{4+} than Zn^{2+}, these high valence metal cations preferentially adsorb onto the surface of metallic zinc, shielding parasitic reactions between zinc and electrolyte, reshaping the electric filed distribution, and directing preferential homogeneous deposition of Zn-ions on the Zn (002) crystal plane. Furthermore, the adsorption of Zr^{4+} can on the Zn metal after electrochemical cycles and enhance the energy barrier of zinc atom diffusion, resulting in high resistance of corrosion and manipulation of Zn^{2+} nucleation configuration. Attributing to these properties, the Zn//Zn symmetric cell with electrolyte additive of ZA was able to cycle for 400 h under an extreme high current density of 40 mA cm^{-2} with an area capacity of 2 mAh cm^{-2}. Meanwhile, MnO_2//Zn coin cell still had 81.7 mAh g^{-1} (85 % retention of capacity) after 850 cycles under a current density of 1 A g^{-1}.

Introduction

Aqueous zinc-ion batteries (AZIBs) are the most promising next-generation large-scale energy storage device due to high safety and low cost of aqueous electrolyte. Meanwhile, metal zinc anodes stand out from the rest with their high safety and high theoretical specific capacity (820 mAh g^{-1} and 5855 mAh cm^{-2}), as well as the abundance of reserves in the earth.[1–4] In spite of so many perfect advantages of AZIBs, the cycling lifetime of AZIBs is still limited due to the formation of zinc dendrites continuous electrochemical corrosion between zinc anode and aqueous electrolyte. The corrosion will induce the hydrogen evolution reaction (HER) and forming an inert layer on the surface of zinc anode with the main composition of $Zn_4SO_4(OH)_6 \cdot xH_2O$ (ZHS), strongly shortening the cycling life.[5] These phenomena will be intensified when the high current density applied. Therefore, it is a challenge to achieve a highly stable AZIBs under high-rate conditions.

Against this background, researchers have proposed many different strategies such as zinc alloys anode, electrolyte modification into gels and electrolyte additive optimization to strengthen the cycling stability of AZIBs.[6–8] For example Yang *et al.*

the zinc-phosphorus alloy coated zinc foil was used as the anode of AZIBs (Zn@ZnP), in which the P atoms facilitated the reduction of the electrochemical activation energy and accelerated the rapid transfer of ions during Zn stripping/plating, enhancing the cycling lifetime of AZIBs under high-rate conditions.[9] Guo *et al.* proposed to synthesis a biocompatible hydrogel electrolyte from hyaluronic acid. The hydrogel electrolyte with ample hydrophilic functional groups offers zinc anodes excellent anti-corrosion ability and regulates zinc nucleation/growth.[10] Although all of these strategies can improve the performance of AZIBs, most of these strategies are still costly and preparation complicated, which are limited in the commercial production. In comparison, modification of electrolyte such as electrolyte additives could be an economical and effective strategy to stabilize the zinc anode.

State of art, numerous electrolyte additives are widely proposed to enhance the cycling stability of AZIBs, which are mainly acid or organic compounds. These additives improve the cycling lifetime of AZIBs significantly *via* PH buffer effect, constructing a stable SEI or electrostatic shielding layer and improve the migration of Zn^{2+} in the aqueous electrolyte.[11–13] Nevertheless, it is still challenged for achieving high-rate AZIBs as the intensive formation of zinc dendrites under the high rate. Recently, the deposition of Zn^{2+} on Zn (002) crystal plane is widely reported to maintain electrochemical stability.[8,14,15] Considering the uncertainty of Zn^{2+} deposition on the surface of metallic zinc, adding electrolyte additives to direct deposition of Zn-ions on the Zn (002) crystal plane after stripping/plating may be an effective method to stabilize AZIBs for long cycling under extreme high currents.

Here in, a liquid metal acetate of zirconium acetate (ZA) was added to the original $ZnSO_4$ electrolyte of AZIBs. Attributing to the higher electro-positivity of Zr^{4+} than Zn^{2+}, these high valence metal cations can preferentially adsorb onto the Zn anode surface, shielding the parasitic reaction between zinc and electrolyte, reshaping the electric filed distribution, and directing the preferential homogeneous deposition of Zn^{2+} on the Zn (002) crystal plane (Figure 1a). Specifically, the Zr^{4+} be adsorbed on the

surface of Zn metal and enhance the energy barrier of Zinc atom diffusion (from 0.037 eV to 0.053 eV), resulting in the resistance of corrosion and manipulation of the Zn^{2+} nucleation configuration. Impressively, with the addition of ZA, the Zn//Zn symmetric cell was able to cycle for more than 1800 hours under a current density of 5 mA cm^{-2} with an area capacity of 1 mAh cm^{-2} and for more than 400 hours even under the extreme high current density of 40 mA cm^{-2} and an area capacity of 2 mAh cm^{-2}. The Zn electrode in the ZA modified electrolyte has an excellent plating/stripping reversibility and an average Coulombic efficiency of 99.21 % after 400 cycles. The MnO_2//Zn full cell still had a capacity of 81.7 mAh g^{-1} (85 %) after 850 cycles under a high current density of 1 A g^{-1}. The study verifies the introduction of Zr^{4+} ions into the electrolyte can effectively inhibit the dendrite growth by contributing to a uniform deposition of Zn^{2+}. This strategy paving a new pathway for developing aqueous electrolyte used in high rate AZIBs.

Results and discussion

Liquid metal acetate (ZA) was chosen as electrolyte additives in 2 M $ZnSO_4$ original electrolyte of AZIBs. Density functional theory (DFT) calculations was used firstly to verify the absorption ability of Zr^{4+} on the surface of metallic zinc surface, where the adsorption energy of Zr^{4+} on Zn (002) crystal plane (-4.8 eV) was much higher than H_2O and Zn^{2+}(-0.08 eV and -0.24 eV) (Figure 1b, S1), suggesting that Zr^{4+} would be preferentially adsorbed on the surface of the metallic zinc anode than water molecules. Furthermore, the adsorption energy of Zr^{4+} on different crystal plane of Zn metal were also compared and the adsorption energy on the Zn (002) crystal plane was lowest than that on the Zn (001) crystal plane and Zn (101) crystal plane (-4.8 eV, -6.3 eV and -5.44 eV) (Figure 1c, S2). This suggests that Zr^{4+} is preferentially adsorbed on the Zn (100) and Zn (101) crystal planes, guiding the deposition on the Zn (002) crystal plane.[16] The results indicated that Zn^{2+} tends to be preferentially deposited on the Zn(002) crystal plane with the addition of Zr^{4+}, which can subsequently promote the uniform deposition of zinc-ions during the cycling.[12,17] Furthermore, the as-formed Zn-

Zr^{4+} interface will shield the water molecules from the Zn surface and protect it from the further side reaction.[18] The effect of ZA additives also changes properties of 2 M $ZnSO_4$ electrolyte, which were examined by experimental methods.

To begin with, different volume of liquid ZA was added to 2 M $ZnSO_4$ electrolyte (Figure S3), which were then used to fabricate Zn//Zn symmetric cells and test the rate performance (from 1 to 15 mA cm^{-2}). The results show that the lower the ZA content,

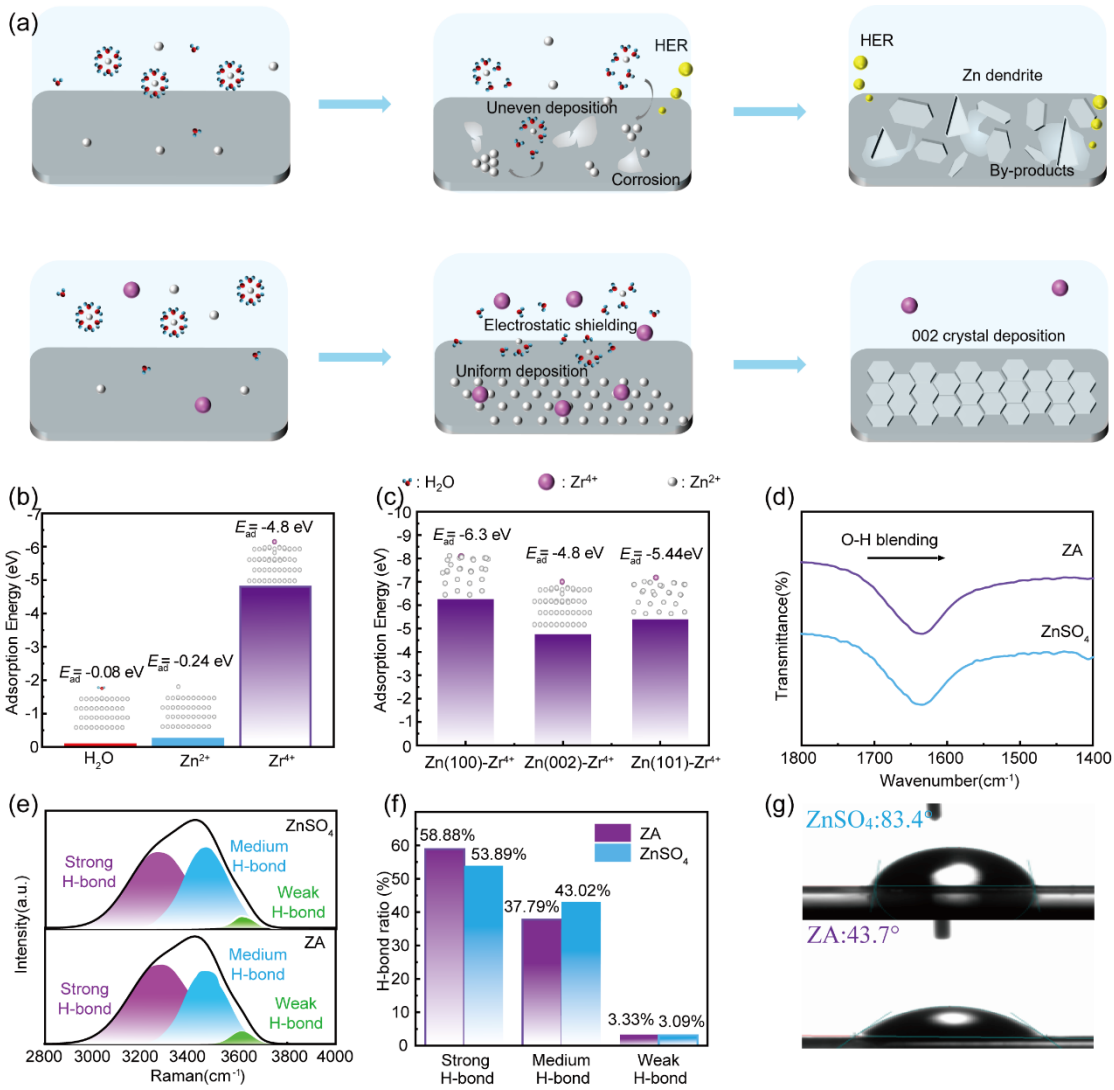

Figure 1 Schematic diagram electrolyte additives for ZA and theoretical calculations for Zr^{4+} on Zn deposition and diffusion behaviors. a) Schematic of Zn^{2+} deposition in the $ZnSO_4$ electrolyte and the ZA electrolyte ($ZnSO_4$ +25 μL). b) Adsorption energy of H_2O, Zn^{2+} and Zr^{4+} on Zn (002) crystal plane. c) Absorption energy comparison of Zr^{4+} on different Zn crystal planes. d) FT-IR spectra for ZA and $ZnSO_4$ electrolytes of O-H blending. e) Raman spectra for ZA and $ZnSO_4$ electrolytes within the region of O-H stretching vibration. d) Corresponding the proportions of strong, medium, and weak H-bond in different electrolytes. g) Contact angle test of different electrolytes.

the lower overpotential in the rate curve (Figure S4). Therefore, 2 M $ZnSO_4$ electrolyte with addition of 25 μL ZA (ZA) was assumed to be the optimal formulation and taken as an example to be compared with the original electrolyte ($ZnSO_4$) in the following characterization and electrochemical tests. The addition of ZA optimizes the solvation structure of Zn^{2+} during the transportation and inhibit the side reaction between zinc and electrolyte. The transformation of -OH bonds in the mixed solution after the addition of ZA additive to the $ZnSO_4$ electrolyte was experimentally investigated using Fourier transform infrared (FT-IR) and Raman spectral.[19] With the addition of the ZA additive, the vibration bands of O-H stretching shows a shift from 1634.53 to 1634.56 cm^{-1} while the O-H blending vibration bonds shows a sightly increase 3226.62 to 3227.46 cm^{-1}(Figure 1d, S5 and S6)[20–22]. The variation is resulting from the destruction of the H-bond network of H_2O due to the weak interaction between lone pair electrons on O of OH groups and ZA molecules.[17] The same shift vibrations were verified in Raman spectra, which shows typical strong, medium, and weak hydrogen bonding peaks at 3250 cm^{-1}, 3500 cm^{-1} and 3600 cm^{-1}, respectively (Figure 1e). Based on Raman spectra to calculate the hydrogen bonding content of different electrolytes (Figure 1f), the ZA additive significantly enhanced the content of strong hydrogen bonding (58.88 % *vs.* 53.89 %) and the content of weak hydrogen bonding remained basically stable compared to the $ZnSO_4$ electrolyte, suggesting that the addition of the ZA can release the bound H_2O fraction into the electrolyte, reduce the H_2O activity and inhibit the active side reaction between H_2O and zinc electrode.[8,21,23] The wettability between the electrolyte and the metallic zinc foil was evaluated by contact angle experiments, where the contact angle was increased from 83.4 ° to 43.7 ° with the addition of the ZA additive (Figure 1g), indicating a better diffusion of Zn^{2+} from electrolyte to zinc foil.[24]

Apart from the adjusting the solvation structure of Zn in the electrolyte, the addition of ZA in $ZnSO_4$ electrolyte is also beneficial to Zinc deposition and anticorrosion as the as-absorbed Zr^{4+} could reshaping the electric filed distribution and directing the preferential homogeneous deposition of Zn^{2+} on the Zn (002) crystal

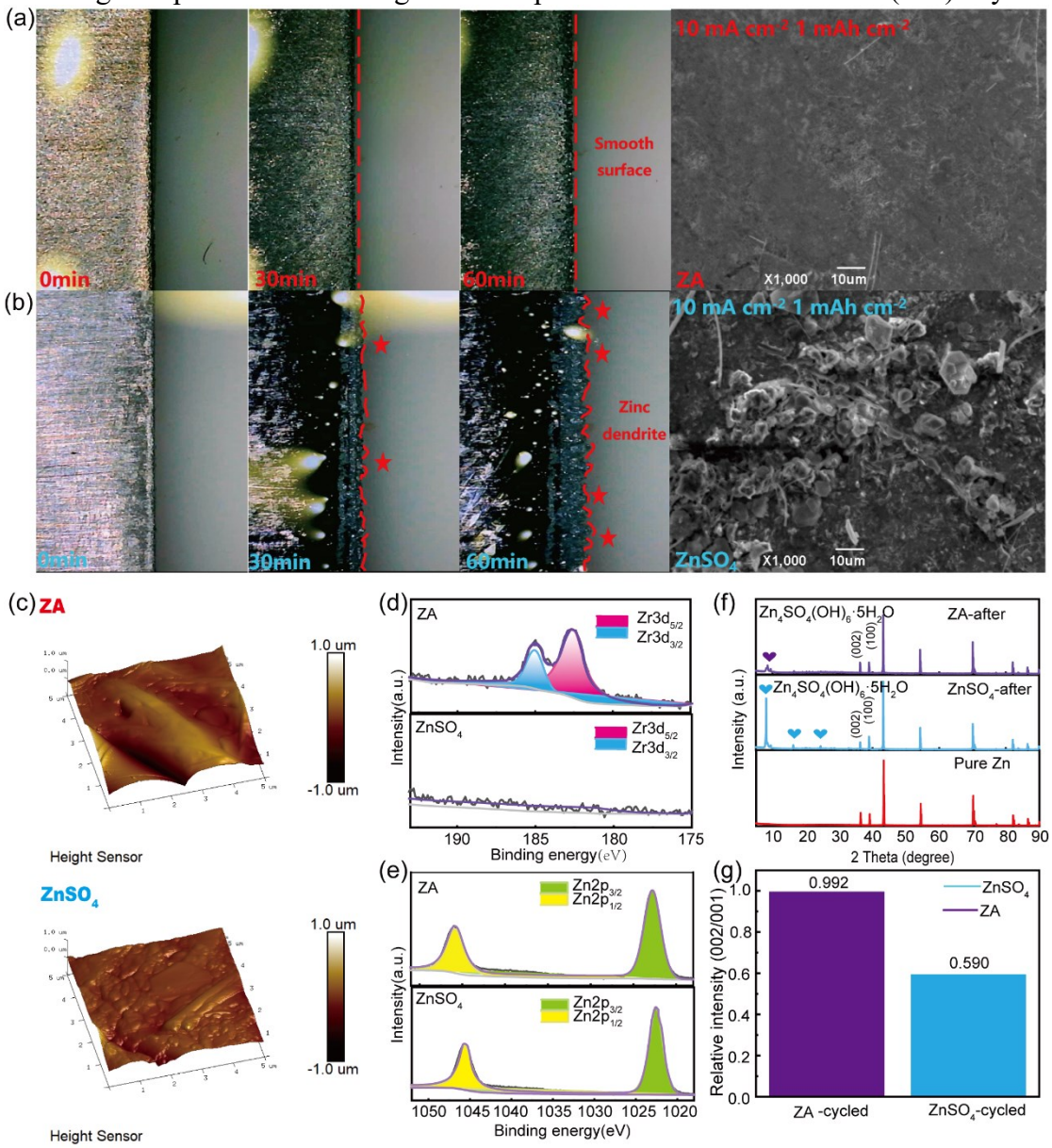

Figure 2. Zn deposition morphologies in the ZA and $ZnSO_4$ electrolyte. In-situ optical microscopy images of the Zn plating in a) Upper left the ZA electrolyte and b) Lower left $ZnSO_4$ electrolyte at 10 mA cm^{-2} 1 mAh cm^{-2}. SEM images of Zn deposition with condition of 10 mA cm^{-2} 1 mAh cm^{-2} in a) Upper right ZA electrolyte and b) Lower right $ZnSO_4$ after 100 cycles. AFM images of the Zn foil surface after cycled in c) ZA electrolyte and $ZnSO_4$ electrolyte at 5 mA cm^{-2} 1 mAh cm^{-2}. d) Zr and e) Zn XPS image of the Zn foil surface after cycled in different electrolytes. f) XRD patterns of Zn//Zn symmetric cells after cycled in the ZA and $ZnSO_4$ electrolytes. g) Zn (002)/Zn (001) ratio of ZA-cycled and $ZnSO_4$-cycled.

plane.[20,25,26] The inhibition effect of Zr^{4+} ions on zinc dendrites was firstly visualized by *in-situ* optical microscopy, which can be used to clearly observe the dendrite growth located at the cross-section of the Zn electrode.[27] As shown in Figure 2a and 2b, no formation of Zn dendrites was detected in the ZA electrolyte after cycling at 10 mA cm^{-2} and 1 mAh cm^{-2} for 1 hour. The cross-section of the electrode remained flat, suggesting the homogeneous deposition of Zn deposition. On the contrary, the cross-section of electrode with $ZnSO_4$ electrolyte was already covered by irregular Zn dendrites after cycling under the same conditions and the same time. A more distinct comparison can be obtained by comparing the whole process of zinc deposition. Scanning electron microscopy (SEM) was then performed to investigate how the electrolyte affected the Zn plating behavior.[28] The electrode taken from ZA electrolyte-based cell showed a smooth and flat surface. In contrast, the electrode taken from $ZnSO_4$ electrolyte-based cell shows a rough and uneven surface, with visible Zn dendrites formed. The similar phenomenon can also be obtained from the electrode cycled for other conditions (Figure S7). Moreover, atomic force microscopy (AFM) images also showed that the surface roughness of the Zn electrode cycled in ZA electrolyte was much less than that of the $ZnSO_4$ electrolyte. (Figure 2c). Furthermore, the composition of the zinc foil surface was investigated by X-ray photoelectron spectroscopy (XPS) and X-ray diffraction patterns (XRD). The XRD pattern proved that the addition of ZA can significantly inhibit the formation of side-products (ZHS) (Figure 2f). Electrodes after cycled in ZA electrolyte shows a higher ratio of Zn (002) to (100) than $ZnSO_4$ one (0.992 *vs.* 0.590), indicating the additive also contribute to the uniform deposition of zinc along 002 crystal plane (Figure 2g). The appearance of Zr $3d_{5/2}$, $3d_{3/2}$ peaks proves that Zr^{4+} exists on the surface of zinc foils (Figure 2d), Meanwhile, the peaks of Zn $2p_{1/2}$ is shifted left obviously (from 1045.4 ev to 1046.1 ev), suggesting Zinc was slightly oxidized and could be evidence that Zr^{4+} was adsorbed on the Zn metal surface. It can be concluded that the introduction of high-valent metal Zr^{4+} ions can significantly promote the unform deposition of zinc and prohibit the

formation of zinc dendrites. Energy Dispersive X-ray Spectroscopy (EDS) mapping similarly demonstrated that Zr^{4+} was not inserted into the zinc anode, but rather adsorbed on the surface (Figure S8, Table S1).

Such signification improvement on dendrites inhibition was subsequently explained by chronoamperometry (CA) tests (Figure 3a). With the addition of Zr^{4+}, the CA curve shows a short two-dimensional diffusion and followed by a much stabler three-dimensional diffusion, leading to a uniform deposition.[17] In comparison, the original $ZnSO_4$ electrolyte always exhibits a two- dimensional diffusion, which induce the Zn dendrites and requires more time and higher current density to be stabilized for

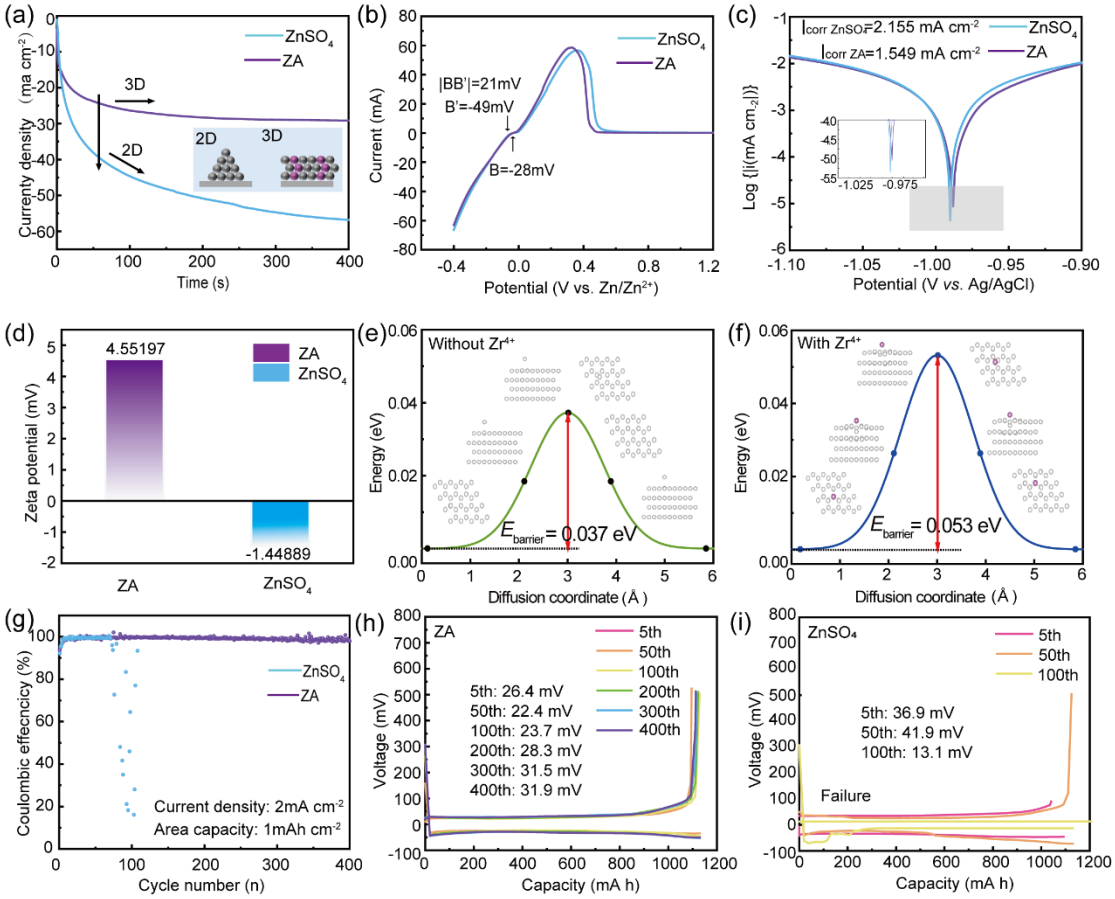

Figure 3 Characterization of properties of different electrolytes. a) The CA curves for Zn//Zn symmetrical with various electrolytes. b) Nucleation overpotential of Zn//Ti asymmetrical cells in the ZA and $ZnSO_4$ electrolytes with a scan rate of 10 mV S^{-1}. c) Linear polarization curves of the Zn foil in the ZA and $ZnSO_4$ electrolytes at 5 mV S^{-1} using a three-electrode system. d) Zeta potential of Zn electrode with different electrolytes. The Zn migration energies on Zn crystal plane (e) without Zr^{4+} and (f) with Zr^{4+}. g) Coulombic efficiency of Zn//Cu symmetric cells under condition 2 mA cm^{-2} and 1 mAh cm^{-2} in different electrolytes. The corresponding charge/discharge curves of Zn//Cu cells in h) the ZA electrolyte and i) the $ZnSO_4$ electrolyte.

Zn even growth.[29–31] Linear scanning voltammetry (LSV) was performed to examine the process of improved charge transfer and homogeneous deposition. The onset of Zn plating in ZA electrolyte was higher than that of $ZnSO_4$ (Figure 3b), suggesting that the addition of ZA lowered the Zn nucleation barrier. In order to test the activity of the HER, different electrolytes were employed in a three-electrode system (Pt electrode as the working and counter electrode and Ag/AgCl electrode as the reference electrode). The onset potential for the HER was found to be higher than that of $ZnSO_4$ in ZA electrolyte (-1.03872 V *vs.* -1.02953 V), which had a significant inhibitory effect on the HER (Figure S9).[31–33] To investigate the effect of ZA additive on the reversibility of Zn plating/stripping, asymmetric Zn//Cu cells based on both electrolytes were fabricated and tested under a current density of 2 mA cm^{-2} with a capacity of 1 mAh cm^{-2}.[19,34,35] Zn//Cu in $ZnSO_4$ electrolyte was only cycled for less than 100 cycles and had a relatively lower coulombic efficiency, which was attributed to the growth of dendrites on the surface of the Zn anode and the generation of by-products (eg. ZHS).[36] In opposite, the ZA electrolyte cycled up to 400 cycles under the same conditions and achieved an average coulombic efficiency of 99.21 % (Figure 3g). Meanwhile, Comparing the overpotentials of Zn//Cu cells at different number of cycles of the two electrolytes, the overpotential of ZA electrolyte remained stable from 26.5 mV in the 5^{th} to 31.9 mV in the 400^{th} cycle, which is much lower than that of $ZnSO_4$ electrolyte (36.9 mV in the 5^{th} to 13.1 mV in the 100^{th}), it was already shorted out at the 100^{th}. And the voltage hysteresis of the different cycles of Zn//Cu cells based on the ZA electrolyte is always lower than that of the $ZnSO_4$ electrolyte, demonstrating significantly more uniform Zn deposition, suppressed side reactions and thus excellent reversibility (Figure 3h, 3i).[37]

These properties of Zn electrochemical deposition suggest the significant inhibition contributed by Zr^{4+}. In addition to the shield of side reaction discussed above, the significant improvement can also be attributed to absorption of Zr^{4+} in zinc electrode during the cycles, which has been proved in XPS results (Figure 2d and e). DFT

calculation was performed to compare the diffusion barrier of Zn atom on the zinc surface with and without Zr^{4+}, where the front shows a higher energy barrier of 0.053 eV than that of later one, which is 0.037 eV. (Figure 3e and f). Such effect will provide zinc anode the resistance of corrosion. The DFT calculations are consistent with our electrochemical results shown above. Additionally, the Tafel currents of ZA and $ZnSO_4$ electrolytes were measured using the three-electrode system to verify the corrosion resistance of zinc foil in two electrolytes (Figure 3c). The corrosion current of zinc electrode in ZA electrolyte (1.549 mA cm^{-2}) is much lower than that of $ZnSO_4$ (2.155 mA cm^{-2}), indicating that the introduction of ZA inhibits the corrosion of zinc electrode significantly.[31,38] The promotional effect of ZA additives on the deposition of Zn^{2+} was examined by comparing the zeta potentials of the zinc metal after plating Zn with different electrolytes. As shown in Figure 3d, the addition of ZA in $ZnSO_4$ electrolyte increased the zeta potential of zinc electrodes from -1.44889 mV to 4.55197 mV. The higher positive potential can provide the Zn surface a strong electrostatic shielding effect and induce the uniform Zn deposition, which is consistent with our DFT calculation (Figure 1b).

The electrochemical stability of Zn electrodes in $ZnSO_4$ and ZA electrolytes was further compared in a Zn//Zn symmetric cell. As expected, the cycle life of Zn//Zn of ZA electrolyte at different current densities is much higher than that of $ZnSO_4$ electrolyte. The cell with ZA electrolyte reached a cycle life of over 1800 h at current density of 5 mA cm^{-2} and area capacity of 1 mAh cm^{-2}, while the cell based on the $ZnSO_4$ electrolyte short-circuited after only less than 280 h of cycling under the same conditions (Figure 4a).[39,40] By comparing the cycle voltage distributions of the 1^{st}, 500^{th}, 1000^{th}, 1500^{th} and 2000^{th} cycles of the ZA electrolytes, it can be clearly observed that the overpotential of the Zn//Zn symmetric cell with ZA electrolyte deliver excellent stability throughout such long cycles. However, the cell with $ZnSO_4$ electrolyte has already soft short-circuited at the 725^{th} cycle (Figure 4c). In order to investigate the high-rate capability provided by ZA additives, an extreme high current density of 40

mA cm^{-2} with an area capacity of 2 mAh cm^{-2} was applied. It is noteworthy that the cell with ZA additives exhibits a prolonged cycling time of 400 hours, whereas the original electrolyte cell only survived for less than 100 hours. This highlights the potential of the additives in high-rate batteries. Furthermore, the cycle life of the Zn//Zn symmetric cell is found to be significantly shorter than that of the 25 μL ZA electrolyte, with a duration of only 230 h and 120 h, respectively. This evidence directly

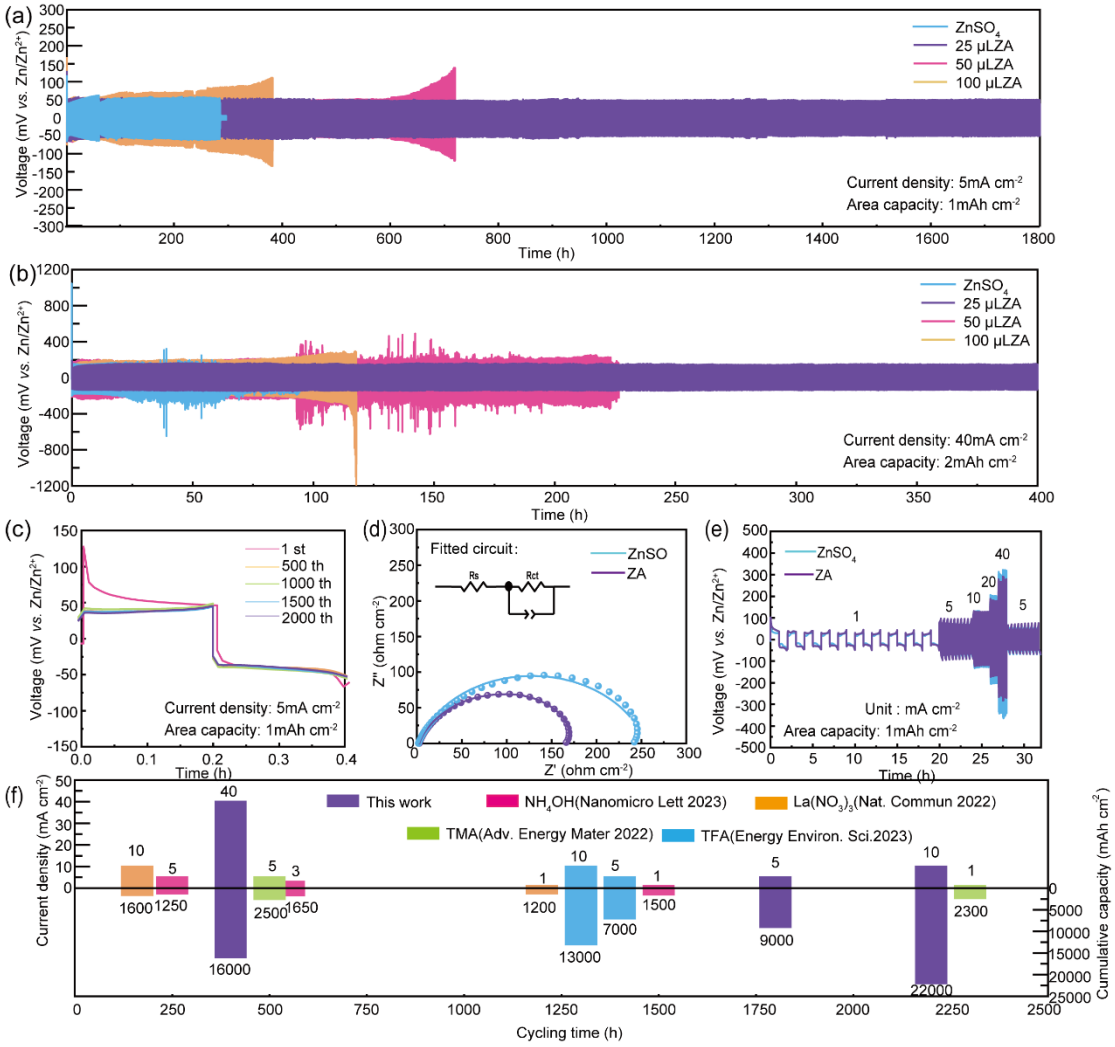

Figure 4. Electrochemical performance of the Zn//Zn symmetric cell in the $ZnSO_4$ and ZA electrolyte. a) Long cycling performance of Zn//Zn cell in various electrolytes under cycle condition of 5 mA cm^{-2} 1 mAh cm^{-2}. b) Long cycling performance of Zn//Zn cell in various electrolytes under cycle condition of 40 mA cm^{-2} 2 mAh cm^{-2}. c) The comparison of overpotentials in ZA electrolyte at 5 mA cm^{-2} 1mAh cm^{-2} with different cycles. d) Nyquist plots the Zn//Zn full cell in the $ZnSO_4$ and ZA electrolyte. The insert figure is fitted circuit of Zn//Zn full cell. e) Rate performance of Zn//Zn full cell at densities from 1 to 40 mA cm^{-2} in various electrolytes. f) The comparison of electrochemical performance with other reported literatures.

substantiates the assertion that 25 μL ZA is the optimal electrolyte (Figure 4b). Meanwhile, other testing conditions were used to verify the reliability of the improvement, in which the same conclusion were obtained (Figure S10, S11 and S12). To demonstrate that the battery based on additives can function under higher area capacity conditions, it was raised to 5 mAh cm^{-2}. Gradually increasing the current density from 10 mA cm^{-2} to 40 mA cm^{-2}, the cycle life of Zn//Zn symmetric cells containing ZA additives were all higher than that of the $ZnSO_4$ electrolyte. It is demonstrated the wide practical range of ZA additives, which can be effective at both high current densities and area capacities (Figure S13). In addition, the rate performance of Zn//Zn symmetric cells with different electrolytes was compared by gradually increasing the current density from 1 to 40 mA cm^{-2} at a fixed area capacity of 1 mAh cm^{-2}. At all current densities, the cells with ZA electrolyte exhibited lower overpotentials and the reduced internal resistance (Figure 4e). The stabilizing effect of the two electrolytes on the zinc anode was tested by setting the maximum current density of the Zn//Zn symmetric cell to 50 mA cm^{-2} and the area capacity to 2 mAh cm^{-2}. The cell based on ZA electrolyte cycle life up to 70 hours, in contrast to less than 30 hours for the $ZnSO_4$ electrolyte (Figure S14). It is also consistent with the electrochemical impedance spectrum (EIS) (Figure 4d).[41] The electrolyte additive in this work is compared with other reported electrolyte additives considering current density, cycle life and the area capacity, showing the outstand improvement of ZA additives (Figure 4f , Table S4).[1,15,48,49,24,25,42–47]

To demonstrate the feasibility of ZA in practical applications, MnO_2//Zn full cells were assembled according to Figure S15. The XRD patterns of commercial MnO_2 are shown in Figure S16. The cyclic voltammetry (CV) curves of MnO_2//Zn full cells in different electrolytes (Figure 5a) with a scan rate of 0.5 mV S^{-1} show similar redox peaks, indicating that the ZA additive does not affect the electrochemical charge storage

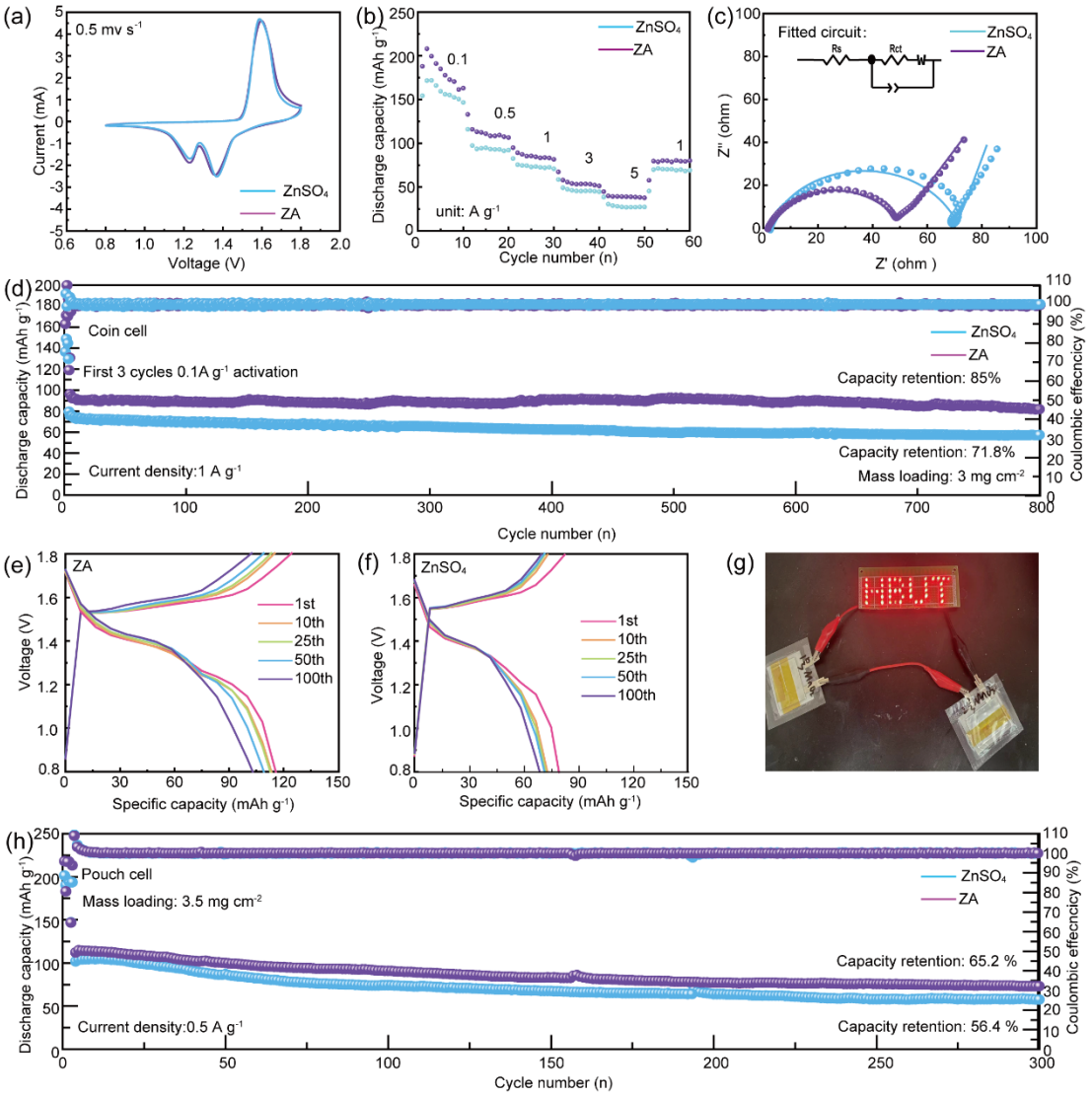

Figure 5. Electrochemical performance of the MnO_2//Zn full cell in the $ZnSO_4$ and ZA electrolytes. a) The CV curves of MnO_2//Zn full cell at 0.5 mV S^{-1} in different electrolytes. b) Rate performance of MnO_2//Zn full cell at densities from 0.1 to 5 A g^{-1} in various electrolytes. c) Nyquist plots of the MnO_2//Zn full cell in the $ZnSO_4$ and ZA electrolyte. The insert figure is fitted circuit of MnO_2//Zn full cell. d) Long cycling performance of MnO_2//Zn full cell in various electrolytes at 1 A g^{-1}. The charging/discharging curves obtains from the cycling tests at different cycles in e) ZA and f) $ZnSO_4$ electrolyte. g) Practical application of pouch cells to light up LEDs. h) Cycling performance of MnO_2//Zn pouch cells with different electrolyte.

mechanism of MnO_2.[50] Furthermore, the rate performance of the full cells was investigated in the range of 0.1 A g^{-1} to 5 A g^{-1}, where the specific capacity of the MnO_2//Zn full cells based on the ZA electrolyte was higher than that of the $ZnSO_4$ electrolyte at all current densities, especially at high current densities. Such improvement can be attributed to the better diffusion kinetics provided by ZA additives. The better kinetics can also be indicated by impedance spectroscopy, which demonstrated the resistance of the MnO_2//Zn full cell based on the ZA electrolyte was lower than that of the $ZnSO_4$ electrolyte (Figure 5c).

Subsequently, a comparison of the long-cycle stability of cells based on different electrolytes was performance under a current density of 1 A g^{-1} (Figure 5d), in which the cell with ZA electrolyte was able to deliver a reversible capacity of 96.1 mAh g^{-1}, with a capacity retention rate of 85 % (81.7 mAh g^{-1}) after 850 cycles. In contrast, the cell with $ZnSO_4$ electrolyte only exhibited a low capacity of 49.76 mAh g^{-1} after 850 cycles. The galvanostatic charge-discharge (GCD) curves of the two electrolytes were compared at the 1^{st}, 10^{th}, 25^{th}, 50^{th}, and 100^{th} cycles (Figure 5e and 5f). The specific capacity of the cell with ZA electrolyte was showing a flatter discharge and charge plateau and a better reversibility than that with $ZnSO_4$ electrolyte. Similar results were also obtained when current density was changed to 0.5 A g^{-1} (Figure S17). In addition, the electrochemical performance of the MnO_2//Zn full cell was tested under more practical conditions (high mass loading of MnO_2). By increasing the mass of the active substance at the cathode to 6 mg cm^{-2}, the capacity of the full cell with ZA electrolyte was still 93.62 mAh g^{-1} after 200 cycles, with a capacity retention of 90.6 %. In contrast, the capacity retention of the $ZnSO_4$ electrolyte was only 77.5 % (Figure S18). The CV of MnO_2//Zn full cells assembled with different electrolytes at different scanning speeds are shown in Figure S19a and c. The Zn^{2+} diffusion coefficients for different systems can be calculated by the Randles-Sevcik formula (Equation S1). The electrochemical kinetics in different electrolytes were described by showing the linear relationship between Ip and $V^{1/2}$ (Figure S19b and d). The calculations showed that the Zn^{2+}

diffusion coefficient was enhanced after the addition of ZA additive (Figure S19e). These results demonstrate the introduction of the ZA additive can promotes the Zn^{2+} reaction kinetics in full cells, enhancing the reversible capacity and long-term cycling stability of the full cell. The possibility of practical application was further evaluated by assembling a MnO2 pouch cell.[51] Two pouch cells based on ZA electrolyte successfully lit up an LED light sign with a voltage of 3V (Figure 5g). The pouch based on ZA electrolyte provided higher specific capacity and close to 100% CE in the long cycle test of the pouch batteries with both electrolytes. Compared to the $ZnSO_4$ electrolyte, the capacity retention is improved, although the specific capacity improvements are not significant. (Figure 5h), indicating that the addition of ZA electrolyte has great potential for practical applications.

Conclusions

In summary, high valence metal ions of Zr^{4+} were introduction into $ZnSO_4$ electrolyte for aqueous zinc ion batteries. Both experiments and theoretical calculations show that the electro-positivity metal Zr^{4+} ions are preferentially adsorbed on the Zn (002) crystal plane, which shields the side reaction between zinc and electrolyte, reshapes the electric filed distribution, and directs the preferential homogeneous deposition of Zn^{2+} on the Zn (002) crystal plane. In addition, Zr^{4+} was adsorbed on the zinc metal surface during the cycles, which raises the diffusion energy barrier of zinc atoms (from 0.037 eV to 0.053 eV), improving the corrosion resistance of the zinc foil and further inhibiting the growth of zinc dendrites. Owing to these characteristics provided by ZA additives, the Zn//Zn symmetric cell was able to cycle for more than 1800 hours at a current density of 5 mA cm^{-2} with an area capacity of 1 mAh cm^{-2} and for more than 400 hours even under the extreme high current density of 40 mA cm^{-2} and an area capacity of 2 mAh cm^{-2}. The Zn electrode in the ZA modified electrolyte has an excellent plating/stripping reversibility and an average Coulombic efficiency of 99.21 % after 400 cycles. The MnO_2//Zn full cell still had a capacity of 79.4 mAh g^{-1} (82.6 %) after 850 cycles under

a high current density of 1 A g^{-1}. The strategy paving a new pathway for developing aqueous electrolyte used in high rate AZIBs.

Supporting Information

Details on preparation of the electrolyte, cathode, electrochemical testing and various characterizations. Calculations method and long cycles at different current densities. A table of electrochemical performance comparison with other electrolytes in reported literatures.

Conflicts of interest

The authors declare no conflict of interest.

Acknowledgements

This work was funded by the Startup fund at Hubei University of Technology, and High-level talent grant of Hubei province.

Data availability

Data will be made available on request.

References

(1) Bayaguud, A.; Luo, X.; Fu, Y.; Zhu, C. Cationic Surfactant-Type Electrolyte Additive Enables Three-Dimensional Dendrite-Free Zinc Anode for Stable Zinc-Ion Batteries. *ACS Energy Letters* **2020**, *5* (9), 3012–3020. https://doi.org/10.1021/acsenergylett.0c01792.

(2) Xu, J.; Lv, W.; Yang, W.; Jin, Y.; Jin, Q.; Sun, B.; Zhang, Z.; Wang, T.; Zheng, L.; Shi, X.; Sun, B.; Wang, G. In Situ Construction of Protective Films on Zn Metal Anodes via Natural Protein Additives Enabling High-Performance Zinc Ion Batteries. *ACS Nano* **2022**, *16* (7), 11392–11404. https://doi.org/10.1021/acsnano.2c05285.

(3) Yuan, W.; Nie, X.; Wang, Y.; Li, X.; Ma, G.; Wang, Y.; Shen, S.; Zhang, N. Orientational Electrodeposition of Highly (002)-Textured Zinc Metal Anodes Enabled by Iodide Ions for Stable Aqueous Zinc Batteries. *ACS Nano* **2023**, *17* (23), 23861–23871. https://doi.org/10.1021/acsnano.3c08095.

(4) Li, J.; Guo, Z.; Wu, J.; Zheng, Z.; Yu, Z.; She, F.; Lai, L.; Li, H.; Chen, Y.; Wei, L. Dextran: A Multifunctional and Universal Electrolyte Additive for Aqueous Zn Ion Batteries. *Advanced Energy Materials* **2023**, *13* (37), 1–10. https://doi.org/10.1002/aenm.202301743.

(5) Yu, X.; Li, Z.; Wu, X.; Zhang, H.; Zhao, Q.; Liang, H.; Wang, H.; Chao, D.; Wang, F.; Qiao, Y.; Zhou, H.; Sun, S. G. Ten Concerns of Zn Metal Anode for Rechargeable Aqueous Zinc Batteries. *Joule* **2023**, *7* (6), 1145–1175. https://doi.org/10.1016/j.joule.2023.05.004.

(6) Wang, S. B.; Ran, Q.; Yao, R. Q.; Shi, H.; Wen, Z.; Zhao, M.; Lang, X. Y.; Jiang, Q. Lamella-Nanostructured Eutectic Zinc–Aluminum Alloys as Reversible and Dendrite-Free Anodes for Aqueous Rechargeable Batteries. *Nature*

Communications **2020**, *11* (1), 1–9. https://doi.org/10.1038/s41467-020-15478-4.

(7) Hao, Y.; Feng, D.; Hou, L.; Li, T.; Jiao, Y.; Wu, P. Gel Electrolyte Constructing Zn (002) Deposition Crystal Plane Toward Highly Stable Zn Anode. *Advanced Science* **2022**, *9* (7), 1–10. https://doi.org/10.1002/advs.202104832.

(8) Cheng, Y.; Jiao, Y.; Wu, P. Manipulating Zn 002 Deposition Plane with Zirconium Ion Crosslinked Hydrogel Electrolyte toward Dendrite Free Zn Metal Anodes. *Energy and Environmental Science* **2023**, *16* (10), 4561–4571. https://doi.org/10.1039/d3ee02114a.

(9) Cao, P.; Zhou, X.; Wei, A.; Meng, Q.; Ye, H.; Liu, W.; Tang, J.; Yang, J. Fast-Charging and Ultrahigh-Capacity Zinc Metal Anode for High-Performance Aqueous Zinc-Ion Batteries. *Advanced Functional Materials* **2021**, *31* (20), 1–10. https://doi.org/10.1002/adfm.202100398.

(10) Li, G.; Zhao, Z.; Zhang, S.; Sun, L.; Li, M.; Yuwono, J. A.; Mao, J.; Hao, J.; Vongsvivut, J. (Pimm); Xing, L.; Zhao, C. X.; Guo, Z. A Biocompatible Electrolyte Enables Highly Reversible Zn Anode for Zinc Ion Battery. *Nature Communications* **2023**, *14* (1), 1–14. https://doi.org/10.1038/s41467-023-42333-z.

(11) Han, D.; Wang, Z.; Lu, H.; Li, H.; Cui, C.; Zhang, Z.; Sun, R.; Geng, C.; Liang, Q.; Guo, X.; Mo, Y.; Zhi, X.; Kang, F.; Weng, Z.; Yang, Q. H. A Self-Regulated Interface toward Highly Reversible Aqueous Zinc Batteries. *Advanced Energy Materials* **2022**, *12* (9). https://doi.org/10.1002/aenm.202102982.

(12) Li, H.; Yang, L.; Zhou, S.; Li, J.; Chen, Y.; Meng, X.; Xu, D.; Han, C.; Duan, H.; Pan, A. A Self-Regulated Interface Enabled by Multi-Functional PH Buffer for Reversible Zn Electrochemistry. *Advanced Functional Materials* **2024**, *2313859*, 1–9. https://doi.org/10.1002/adfm.202313859.

(13) Huang, C.; Mao, J.; Li, S.; Zhang, W.; Wang, X.; Shen, Z.; Zhang, S.; Guo, J.; Xu, Y.; Lu, Y.; Lu, J. Amphoteric Polymer Strategy with Buffer-Adsorption Mechanism for Long-Life Aqueous Zinc Ion Batteries. *Advanced Functional Materials* **2024**, *2315855*, 1–8. https://doi.org/10.1002/adfm.202315855.

(14) Xu, D.; Chen, B.; Ren, X.; Han, C.; Chang, Z.; Pan, A.; Zhou, H. Selectively Etching-off the Highly Reactive (002) Zn Facet Enables Highly Efficient Aqueous Zinc-Metal Batteries. *Energy and Environmental Science* **2023**. https://doi.org/10.1039/d3ee02522e.

(15) Zhao, R.; Wang, H.; Du, H.; Yang, Y.; Gao, Z.; Qie, L.; Huang, Y. Lanthanum Nitrate as Aqueous Electrolyte Additive for Favourable Zinc Metal Electrodeposition. *Nature Communications* **2022**, *13* (1), 1–9. https://doi.org/10.1038/s41467-022-30939-8.

(16) Hu, S.; Tao, H.; Ma, H.; Yan, B.; Li, Y.; Zhang, L.; Yang, X. Constructing Highly Stable Zinc Metal Anodes via Induced Zn(002) Growth. *ACS Applied Materials and Interfaces* **2024**, *16* (15), 18949–18958. https://doi.org/10.1021/acsami.4c01356.

(17) Deng, Q.; You, S.; Min, W.; Xu, Y.; Lin, W.; Lu, J.; Yang, C. Polymer Molecules Adsorption-Induced Zincophilic-Hydrophobic Protective Layer Enables Highly Stable Zn Metal Anodes. *Advanced Materials* **2024**, *2312924*, 1–10. https://doi.org/10.1002/adma.202312924.

(18) Luo, J.; Xu, L.; Zhou, Y.; Yan, T.; Shao, Y. Y.; Yang, D.; Zhang, L.; Xia, Z.; Wang, T.; Zhang, L.; Cheng, T.; Shao, Y. Y. Regulating the Inner Helmholtz Plane with a High Donor Additive for Efficient Anode Reversibility in Aqueous Zn-Ion Batteries. *Angewandte Chemie* **2023**, *135* (21). https://doi.org/10.1002/ange.202302302.

(19) Qiu, K.; Ma, G.; Wang, Y.; Liu, M.; Zhang, M.; Li, X.; Qu, X.; Yuan, W.; Nie, X.; Zhang, N. Highly Compact Zinc Metal Anode and Wide-Temperature Aqueous Electrolyte Enabled by Acetamide Additives for Deep Cycling Zn Batteries. *Advanced Functional Materials* **2024**, *2313358*, 1–12. https://doi.org/10.1002/adfm.202313358.

(20) Wei, T.; Zhang, X.; Ren, Y.; Wang, Y.; Li, Z.; Zhang, H.; Hu, L. Reconstructing Anode/Electrolyte Interface and Solvation Structure towards High Stable Zinc Anode. *Chemical Engineering Journal* **2023**, *457* (January), 141272. https://doi.org/10.1016/j.cej.2023.141272.

(21) Xie, D.; Sang, Y.; Wang, D. H.; Diao, W. Y.; Tao, F. Y.; Liu, C.; Wang, J. W.; Sun, H. Z.; Zhang, J. P.; Wu, X. L. ZnF2-Riched Inorganic/Organic Hybrid SEI: In Situ-Chemical Construction and Performance-Improving Mechanism for Aqueous Zinc-Ion Batteries. *Angewandte Chemie - International Edition* **2023**, *62* (7). https://doi.org/10.1002/anie.202216934.

(22) Huang, H.; Xie, D.; Zhao, J.; Rao, P.; Choi, W. M.; Davey, K.; Mao, J. Boosting Reversibility and Stability of Zn Anodes via Manipulation of Electrolyte Structure and Interface with Addition of Trace Organic Molecules. *Advanced Energy Materials* **2022**, *12* (38). https://doi.org/10.1002/aenm.202202419.

(23) Li, T. C.; Lim, Y. Von; Li, X. L.; Luo, S.; Lin, C.; Fang, D.; Xia, S.; Wang, Y.; Yang, H. Y. A Universal Additive Strategy to Reshape Electrolyte Solvation Structure toward Reversible Zn Storage. *Advanced Energy Materials* **2022**, *12* (15), 1–9. https://doi.org/10.1002/aenm.202103231.

(24) Li, Y.; Wu, P.; Zhong, W.; Xie, C.; Xie, Y.; Zhang, Q.; Sun, D.; Tang, Y.; Wang, H. A Progressive Nucleation Mechanism Enables Stable Zinc Stripping-Plating Behavior. *Energy and Environmental Science* **2021**, *14* (10), 5563–5571. https://doi.org/10.1039/d1ee01861b.

(25) Chen, R.; Zhang, W.; Huang, Q.; Guan, C.; Zong, W.; Dai, Y.; Du, Z.; Zhang, Z.; Li, J.; Guo, F.; Gao, X.; Dong, H.; Zhu, J.; Wang, X.; He, G. Trace Amounts of Triple-Functional Additives Enable Reversible Aqueous Zinc-Ion Batteries from a Comprehensive Perspective. *Nano-Micro Letters* **2023**, *15* (1), 1–12. https://doi.org/10.1007/s40820-023-01050-4.

(26) Zhang, W.; Dai, Y.; Chen, R.; Xu, Z.; Li, J.; Zong, W.; Li, H.; Li, Z.; Zhang, Z.; Zhu, J.; Guo, F.; Gao, X.; Du, Z.; Chen, J.; Wang, T.; He, G.; Parkin, I. P. Highly Reversible Zinc Metal Anode in a Dilute Aqueous Electrolyte Enabled by a PH Buffer Additive. *Angewandte Chemie - International Edition* **2023**, *62* (5). https://doi.org/10.1002/anie.202212695.

(27) You, C.; Wu, R.; Yuan, X.; Liu, L.; Ye, J.; Fu, L.; Han, P.; Wu, Y. An Inexpensive Electrolyte with Double-Site Hydrogen Bonding and a Regulated Zn2+ Solvation Structure for Aqueous Zn-Ion Batteries Capable of High-Rate and Ultra-Long Low-Temperature Operation. *Energy and Environmental Science* **2023**, *16* (11), 5096–5107. https://doi.org/10.1039/d3ee01741a.

(28) Yang, S.; Chen, A.; Tang, Z.; Wu, Z.; Li, P.; Wang, Y.; Wang, X.; Jin, X.; Bai, S.; Zhi, C. Regulating the Electrochemical Reduction Kinetics by the Steric Hindrance Effect for a Robust Zn Metal Anode. *Energy and Environmental Science* **2023**, *17* (3), 1095–1106. https://doi.org/10.1039/d3ee02164e.

(29) Zhu, J.; Deng, W.; Yang, N.; Xu, X.; Huang, C.; Zhou, Y.; Zhang, M.; Yuan, X.; Hu, J.; Li, C.; Li, R. Biomolecular Regulation of Zinc Deposition to Achieve Ultra-Long Life and High-Rate Zn Metal Anodes. *Small* **2022**, *18* (29), 1–10. https://doi.org/10.1002/smll.202202509.

(30) Luo, M.; Li, T. C.; Wang, P.; Zhang, D.; Lin, C.; Liu, C.; Li, D. S.; Chen, W.; Yang, H. Y.; Zhou, X. Dynamic Regulation of the Interfacial PH for Highly

Reversible Aqueous Zinc Ion Batteries. *Nano Letters* **2023**, *23* (20), 9491–9499. https://doi.org/10.1021/acs.nanolett.3c02904.

(31) Fang, T.; Liu, Q.; Hu, A.; Meng, J.; Fu, Y.; Shi, Z. Dendrite-Free and Stable Zinc-Ion Batteries Enabled by a Cation-Anion Synergistic Regulation Additive. *Journal of Power Sources* **2023**, *581* (August), 233521. https://doi.org/10.1016/j.jpowsour.2023.233521.

(32) Chen, J.; Zhao, W.; Jiang, J.; Zhao, X.; Zheng, S.; Pan, Z.; Yang, X. Challenges and Perspectives of Hydrogen Evolution-Free Aqueous Zn-Ion Batteries. *Energy Storage Materials* **2023**, *59* (April), 102767. https://doi.org/10.1016/j.ensm.2023.04.006.

(33) Cai, Z.; Ou, Y.; Zhang, B.; Wang, J.; Fu, L.; Wan, M.; Li, G.; Wang, W.; Wang, L.; Jiang, J.; Seh, Z. W.; Hu, E.; Yang, X. Q.; Cui, Y.; Sun, Y. A Replacement Reaction Enabled Interdigitated Metal/Solid Electrolyte Architecture for Battery Cycling at 20 MA Cm-2and 20 MAh Cm-2. *Journal of the American Chemical Society* **2021**, *143* (8), 1–16. https://doi.org/10.1021/jacs.0c11753.

(34) Zheng, X.; Liu, Z.; Sun, J.; Luo, R.; Xu, K.; Si, M.; Kang, J.; Yuan, Y.; Liu, S.; Ahmad, T.; Jiang, T.; Chen, N.; Wang, M.; Xu, Y.; Chuai, M.; Zhu, Z.; Peng, Q.; Meng, Y.; Zhang, K.; Wang, W.; Chen, W. Constructing Robust Heterostructured Interface for Anode-Free Zinc Batteries with Ultrahigh Capacities. *Nature Communications* **2023**, *14* (1). https://doi.org/10.1038/s41467-022-35630-6.

(35) Mu, Y.; Li, Z.; Wu, B. ke; Huang, H.; Wu, F.; Chu, Y.; Zou, L.; Yang, M.; He, J.; Ye, L.; Han, M.; Zhao, T.; Zeng, L. 3D Hierarchical Graphene Matrices Enable Stable Zn Anodes for Aqueous Zn Batteries. *Nature Communications* **2023**, *14* (1), 1–14. https://doi.org/10.1038/s41467-023-39947-8.

(36) Zhou, W.; Chen, M.; Quan, Y.; Ding, J.; Cheng, H.; Han, X.; Chen, J.; Liu, B.; Shi, S.; Xu, X. Stabilizing Zinc Deposition through Solvation Sheath Regulation and Preferential Adsorption by Electrolyte Additive of Lithium Difluoro(Oxalato)Borate. *Chemical Engineering Journal* **2023**, *457* (November 2022), 141328. https://doi.org/10.1016/j.cej.2023.141328.

(37) Wan, J.; Wang, R.; Liu, Z.; Zhang, L. L.; Liang, F.; Zhou, T.; Zhang, S.; Zhang, L. L.; Lu, Q.; Zhang, C.; Guo, Z. A Double-Functional Additive Containing Nucleophilic Groups for High-Performance Zn-Ion Batteries. *ACS Nano* **2022**, *17* (January), 1610–1621. https://doi.org/10.1021/acsnano.2c11357.

(38) Chen, J.; Zhou, W.; Quan, Y.; Liu, B.; Yang, M.; Chen, M.; Han, X.; Xu, X.; Zhang, P.; Shi, S. Ionic Liquid Additive Enabling Anti-Freezing Aqueous Electrolyte and Dendrite-Free Zn Metal Electrode with Organic/Inorganic Hybrid Solid Electrolyte Interphase Layer. *Energy Storage Materials* **2022**, *53* (May), 629–637. https://doi.org/10.1016/j.ensm.2022.10.004.

(39) Li, T.; Hu, S.; Wang, C.; Wang, D.; Xu, M.; Chang, C.; Xu, X.; Han, C. Engineering Fluorine-Rich Double Protective Layer on Zn Anode for Highly Reversible Aqueous Zinc-Ion Batteries. *Angewandte Chemie - International Edition* **2023**, *62* (51). https://doi.org/10.1002/anie.202314883.

(40) Liu, Z.; Wang, R.; Ma, Q.; Wan, J.; Zhang, S.; Zhang, L. L.; Li, H.; Luo, Q.; Wu, J.; Zhou, T.; Mao, J.; Zhang, L. L.; Zhang, C.; Guo, Z. A Dual-Functional Organic Electrolyte Additive with Regulating Suitable Overpotential for Building Highly Reversible Aqueous Zinc Ion Batteries. *Advanced Functional Materials* **2023**, *2214538* (5), 1–13. https://doi.org/10.1002/adfm.202214538.

(41) Gou, Q.; Luo, H.; Zhang, Q.; Deng, J.; Zhao, R.; Odunmbaku, O.; Wang, L.; Li, L.; Zheng, Y.; Li, J.; Chao, D.; Li, M. Electrolyte Regulation of Bio-Inspired Zincophilic Additive toward High-Performance Dendrite-Free Aqueous Zinc-

Ion Batteries. *Small* **2023**, *19* (10), 1–12. https://doi.org/10.1002/smll.202207502.

(42) Yao, R.; Qian, L.; Sui, Y.; Zhao, G.; Guo, R.; Hu, S.; Liu, P.; Zhu, H.; Wang, F.; Zhi, C.; Yang, C. A Versatile Cation Additive Enabled Highly Reversible Zinc Metal Anode. *Advanced Energy Materials* **2022**, *12* (2). https://doi.org/10.1002/aenm.202102780.

(43) Wu, M.; Wang, X.; Zhang, F.; Xiang, Q.; Li, Y.; Guo, J. Highly Reversible and Stable Zn Metal Anodes Realized Using a Trifluoroacetamide Electrolyte Additive. *Energy and Environmental Science* **2023**, 21–31. https://doi.org/10.1039/d3ee03040g.

(44) Cai, S.; Hu, J.; Luo, Y.; Zhu, P.; He, T.; Zou, G.; Hou, H.; Ji, X. Hydrophobic Hyamine-Mediated Water-Lean Electric Double Layer Boosting Reversible Dendrite-Free Zinc Metal Anodes. *Advanced Functional Materials* **2024**, *34* (11), 1–11. https://doi.org/10.1002/adfm.202309667.

(45) Yang, Y.; Hua, H.; Lv, Z.; Zhang, M.; Liu, C.; Wen, Z.; Xie, H.; He, W.; Zhao, J.; Li, C. C. Reconstruction of Electric Double Layer for Long-Life Aqueous Zinc Metal Batteries. *Advanced Functional Materials* **2023**, *33* (10). https://doi.org/10.1002/adfm.202212446.

(46) Wang, Z.; Hu, Z.; Ye, M.; Chen, J.; Chen, Y.; Wen, Z.; Zhang, Y.; Tang, Y.; Liu, X.; Li, C. C. Maintaining the Concentration Equilibrium of Proton and Hydroxide Ions by Construction of Bis(2-Aminoethyl)Amine-Based Inner Helmholtz Plane toward Long-Life Zinc Metal Anodes. *Chemical Engineering Journal* **2024**, *481* (December 2023), 148511. https://doi.org/10.1016/j.cej.2023.148511.

(47) Cao, J.; Wu, J.; Wu, H.; Jin, Y.; Luo, D.; Yang, X.; Zhang, L.; Zhang, D.; Qin, J.; Lu, J. Dendrite-Free Zinc Anode via Oriented Plating with Alkaline Earth

Metal Ion Additives. *Advanced Functional Materials* **2024**, *2401537*, 1–10. https://doi.org/10.1002/adfm.202401537.

(48) Yan, T.; Tao, M.; Liang, J.; Zheng, G.; Wu, B.; Du, L.; Cui, Z.; Song, H. Refining the Inner Helmholtz Plane Adsorption for Achieving a Stable Solid-Electrolyte Interphase in Reversible Aqueous Zn-Ion Pouch Cells. *Energy Storage Materials* **2024**, *65* (January). https://doi.org/10.1016/j.ensm.2024.103190.

(49) Zhang, X.; Chen, J.; Cao, H.; Huang, X.; Liu, Y.; Chen, Y.; Huo, Y.; Lin, D.; Zheng, Q.; Lam, K. ho. Efficient Suppression of Dendrites and Side Reactions by Strong Electrostatic Shielding Effect via the Additive of Rb2SO4 for Anodes in Aqueous Zinc-Ion Batteries. *Small* **2023**, *19* (52), 1–8. https://doi.org/10.1002/smll.202303906.

(50) Quan, Y.; Yang, M.; Chen, M.; Zhou, W.; Han, X.; Chen, J.; Liu, B.; Shi, S.; Zhang, P. Electrolyte Additive of Sorbitol Rendering Aqueous Zinc-Ion Batteries with Dendrite-Free Behavior and Good Anti-Freezing Ability. *Chemical Engineering Journal* **2023**, *458* (January), 141392. https://doi.org/10.1016/j.cej.2023.141392.

(51) Wu, Q.; Huang, J.; Zhang, J.; Yang, S.; Li, Y.; Luo, F.; You, Y.; Li, Y.; Xie, H.; Chen, Y. Multifunctional Cellulose Nanocrystals Electrolyte Additive Enable Ultrahigh-Rate and Dendrite-Free Zn Anodes for Rechargeable Aqueous Zinc Batteries. *Angewandte Chemie* **2024**, No. 2. https://doi.org/10.1002/ange.202319051.

TOC Figure

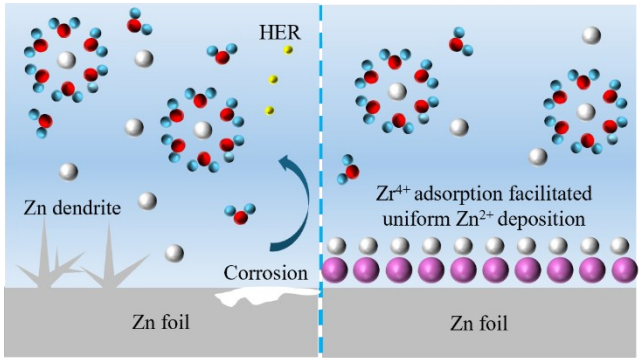
HER
Zn dendrite
Corrosion
Zn foil
Zr4+ adsorption facilitated
uniform Zn2+ deposition
Zn foil